Single-Grasp Object Classification and Feature Extraction with Simple Robot Hands and Tactile Sensors

Adam J. Spiers, *Member, IEEE*, Minas V. Liarokapis, *Member, IEEE*, Berk Calli, *Member, IEEE*, and Aaron M. Dollar, *Senior Member, IEEE*

Abstract—Classical robotic approaches to tactile object identification often involve rigid mechanical grippers, dense sensor arrays, and exploratory procedures (EPs). Though EPs are a natural method for humans to acquire object information, evidence also exists for meaningful tactile property inference from brief, non-exploratory motions (a 'haptic glance'). In this work, we implement tactile object identification and feature extraction techniques on data acquired during a single, unplanned grasp with a simple, underactuated robot hand equipped with inexpensive barometric pressure sensors. Our methodology utilizes two cooperating schemes based on an advanced machine learning technique (random forests) and parametric methods that estimate object properties. The available data is limited to actuator positions (one per two link finger) and force sensors values (eight per finger). The schemes are able to work both independently and collaboratively, depending on the task scenario. When collaborating, the results of each method contribute to the other, improving the overall result in a synergistic fashion. Unlike prior work, the proposed approach does not require object exploration, re-grasping, grasp-release, or force modulation and works for arbitrary object start positions and orientations. Due to these factors, the technique may be integrated into practical robotic grasping scenarios without adding time or manipulation overheads.

Index Terms—Tactile sensing, object classification, object feature extraction, underactuated robot hands, machine learning, adaptive grasping, robotics, haptics applications

1 Introduction

The extraction of object properties or class through both vision and haptic feedback is a natural sensory ability afforded to humans and other animals. In the field of robotics, both sensory modalities have been investigated. Though many properties of objects may be determined visually, common issues of occlusion and/or poor lighting conditions can limit the performance of vision based methods. Furthermore, other physical properties, such as stiffness, are difficult to visually ascertain, particularly without some kind of object manipulation. Regarding haptics, humans are known to make use of various 'exploratory procedures' (EPs) [1], in order to glean object properties through active manipulation of objects by one or both hands. While there have been several robotic approaches that have taken inspiration from this concept (e.g., [2], [3], [4], [5], [6], [7]), such methods tend to rely on time-consuming palpatory motion sequences and robot hand and/or arm dexterity. In various real-world robotic applications (such as industrial pick and place) time or hardware limitations are critical factors that make the use of such EPs inappropriate. Evidence has demonstrated that meaningful knowledge of object properties is acquired by humans during minimal tactile object interactions. Klatzky and Lederman used the term *'haptic glance'* to describe such interactions, which are far simpler than EPs [8]. In turn, the ability of a robot to acquire meaningful haptic knowledge about an object during brief and functional actions may extend the practicality of active tactile sensing into scenarios with limitations on time and/or computational and hardware capabilities. By 'functional actions' we imply actions that serve a goal beyond sensing, such as grabbing an object for transport.

In a similar vein to the above objectives, adaptive underactuated grippers (e.g., Fig. 1) have constituted highly practical robot grasping solutions, with low complexity compared to more traditional approaches. Such systems rely on simple, mechanically adaptive designs (e.g., elastomer flexure joints, tendons and under-actuation) to passively adapt to a wide variety of object shapes and sizes without prior object knowledge, hand modelling, grasp planning, actuator regulation or sensory feedback [9], [10]. These benefits result in a low cost, easily implementable solution to grasping in unstructured scenarios.

In this work we seek to combine the benefits of simple adaptive robot grippers with methods of acquiring meaningful haptic object properties and identifying objects during a single functional grasp via low-cost, commercially available tactile sensors. The resulting method combines parametric estimation and classification (machine learning) techniques, unified via a hybrid collaborative framework (Fig. 2). In previous work we presented some aspects of the classifier alone [11]. Our current work compliments the original classifier via the inclusion of the parametric methods (based on kinematic

• *The authors are with the GRAB Lab, Department of Mechanical Engineering and Materials Science, Yale University, New Haven, CT 06511. E-mail: {adam.spiers, minas.liarokapis, berk.calli, aaron.dollar}@yale.edu.*

Manuscript received 4 June 2015; revised 22 Oct. 2015; accepted 12 Jan. 0000. Date of publication 25 Jan. 2016; date of current version 15 June 2016. Recommended for acceptance by Y. Visell, M. Hartmann, V. Hayward, and N. Lepora. For information on obtaining reprints of this article, please send e-mail to: reprints@ieee.org, and reference the Digital Object Identifier below. Digital Object Identifier no. 10.1109/TOH.2016.2521378

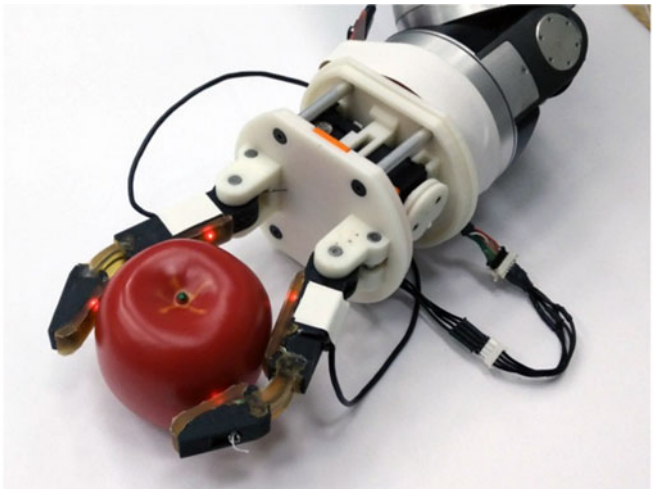

Fig. 1. The adaptive underactuated hand used in this work. Each finger has a proximal pin joint and distal flexor joint, both driven by a single tendon. TakkTile sensors are embedded in the grip pads of each finger.

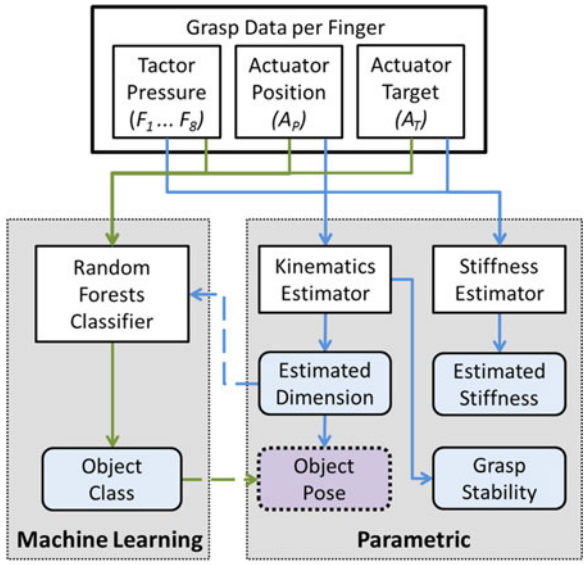

Fig. 2. The collaborative hybrid approach. Machine learning and parametric schemes operate simultaneously during a single, open-loop, object grasp. Outputs have rounded corners.

and stiffness estimation) and a hybrid collaborative approach, where the component outputs support each other to increase overall accuracy in a synergistic fashion (via dynamic classifier retraining and object pose estimation).

Our gripper hardware consists of a simple two-finger underactuated hand equipped with *TakkTile* [12] barometric pressure sensors (Figs. 1 and 4). To maintain consistency with popular open source hand designs [9], the hand does not implement joint position sensing. Our proposed method achieves object classification and object feature extraction using the tactile sensor outputs and actuator positions, measured at three instances of the grasping process.

Taking inspiration from the *haptic glance* concept, our approach does not modify the typical open-loop actuator /finger behavior of adaptive underactuated hands during the grasping process. All necessary computations are also designed to be completed within a short time frame (<100 ms), to allow achievement of the aforementioned goals during a normal grasping process. Overall, the presented process is designed to be executed *during* a single, typical, functional grasp with no temporal or motor overhead. Of course, these constraints (which include uncertain hand kinematics and a single grasp action) significantly reduce data breath, resolution and redundancy compared to more traditional EP based approaches with fully actuated robotic manipulators (e.g., [2], [3], [4]). As a result, state measurement under such conditions is accompanied by a level of uncertainty. However, we believe that some uncertainty is acceptable, given the minimal influence of this method on the fundamental grasping activities carried out daily by thousands of real-world robots. Nevertheless, classifier performance is excellent and parameter estimations are distinct. Though we focus on addressing the problems associated with simple robot hardware and control in this paper, we believe the methods are scalable to more 'complex' robot hands and sensors. For example, greater sensor resolution would only improve the outputs of the proposed algorithms.

An example application where this *haptic glance* philosophy may be useful is the inspection, sorting and packaging of objects (such as fruit) as part of a production line. In this scenario, the proposed methodology could permit the class of object (e.g., apple, pear), stiffness (ripeness), size and pose within the hand to be determined *as* the object is being lifted from the conveyor belt (a functional and necessary manipulation action).

2 Approach

Due to the limited available data (as compared to EP approaches) we propose combining the strengths of two methods of tactile data interpretation via a hybrid approach, the structure of which is illustrated in Fig. 2. This methodology makes use of a random forests (RFs) classifier (a machine learning technique) and parametric object property estimators. The classifier is capable of high level recognition (object class extraction) of different objects based on training data. Conversely, the parametric method aims to provide low-level outcomes related directly to physical object properties of size and stiffness. The two schemes therefore address different aspects of the tactile sensing problem space. Additional cross communication between these two approaches leads to additional parameter determination (object pose within the grasp) and improved classification accuracy. In the latter case, parametrically determined object dimensions are used for class decision validation and dynamic classifier retraining. This retraining process rejects the current class and improves subsequent classification accuracy.

The benefits of the hybrid approach applies to various use cases. For example, remote exploration or disaster response robots may encounter objects with unique and previously unseen characteristics, such as an unusual stone or a fragment of a larger object. While the parametric method may be able to 'measure' such an object, machine learning approaches may have limited classification success due to object novelty compared to training data. Conversely, the machine learning scheme can provide high level identification in structured or semi-structured environments, such as a production line, grocery store or warehouse. Here, encountered objects will always be part of the

company's inventory, though parameter variations in size, stiffness and pose are likely.

The remainder of the paper is structured as follows. First, related literature will be reviewed, focusing on biological then robotic systems. A detailed explanation of experimental conditions and hardware will be described in Section 4. Methods and algorithms of the proposed schemes will be presented in Section 5 with subsequent results in Section 6. Discussion, future work and conclusions will summarize the paper.

3 Related Work

Roboticists have applied tactile sensing to robot hands for many decades, inspired by nature's most versatile end-effector, the human hand. The hand has approximately 17,000 mechanoreceptive units that innervate its skin and provide a highly sophisticated system for understanding the environment [13]. It has been noted that motion of the hand is crucial to fully exploiting its perceptual qualities during physical interaction [1], [13], [14]. Such observations have been reflected in the active-touch approaches of many robot systems. A large proportion of such endeavors make use of complex, high-density sensor systems, such as the multi-modal *BioTac* sensor [15] (used in [3], [4], [6]). This expensive (>$10,000) sensor is capable of providing thermal, vibratory and multiple pressure readings over an anthropomorphic finger pad.

Artificial tactile perception efforts generally focus on either deriving physical object properties or on the higher level discrimination of an object's class. In [13], it was considered that an object's properties contribute to manipulation actions while the object class enables the execution of object specific strategies or plans. Aspects of human tactile object perception will now be discussed.

3.1 Human Haptic Data Acquisition

The ability to characterize and identify objects without reliance on vision is beneficial in a number of scenarios. In humans, common tasks such as reaching for a computer mouse or cup while reading from a computer screen discretely employ complex tactile perceptual methods [8]. Such methods facilitate object understanding (e.g., determining the object class and its pose relative to the hand) and subsequent motor action (orientating the hand to facilitate appropriate use) with limited physical interaction [16]. Studies on more elaborate exploration of objects have demonstrated the ability of humans to identify a large number of objects and properties through touch alone. This is via the use of *exploratory procedures* [1], [14], stereotypical patterns of active hand motions that expose particular physical properties of objects. For example, rubbing permits textural perception, while squeezing exposes stiffness. In medicine, such interactions permit identification of tissue type and underlying structures [17]. It was observed in two finger palpation by surgeons that EPs were often combined [18], permitting multiple feature extraction with increased efficiency.

Investigations have also been made into the capabilities of humans to extract meaningful haptic information with limited active finger/hand motion, which is akin to the single-grasp robotic approach taken in our work. In [8], perceptual accuracy was considered for a 'haptic glance', a brief and restrained contact between fingertips and an object. Similar investigations have been considered with reduced sensory and motor [14], [16], [19] capabilities. Lederman and Klatzky noted that minimal haptic information is often informative enough to lead to object/feature identification and appropriate subsequent manipulation [16]. The methods of this paper explore minimal active touch sensing and motor control in robotic haptic perception. This is realized using data acquired during a non-exploratory 'functional' grasp with adaptive fingers. In [19] it was observed that adaptive 'molding' of the human hand around objects facilitates improved haptic identification. Such 'molding' is fundamental to adaptive grippers.

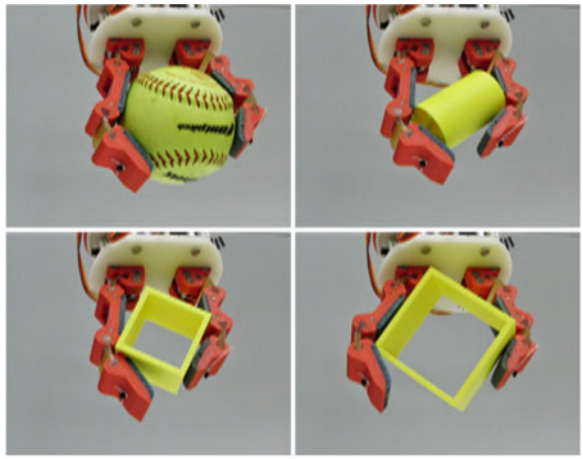

Fig. 3. An *OpenHand T42* securely grasps a variety of objects using open loop motor control with compliant adaptive fingers.

3.2 Adaptive Robot Hands and Tactile Sensing

As previously stated, adaptive underactuated grippers permit grasping of a wide variety of objects with little control or planning effort [20]. This is demonstrated in Fig. 3. In particular, compliant flexure joints permit in-plane finger adaptation to various conditions while maintaining grasp stability [21]. The transmission mechanisms employed in this particular class of hands [9], [10] have similarities to the mechanics and resulting adaptive behavior of the human finger [22].

Despite the benefits of adaptive grippers, there has been relatively limited use of such systems in haptic applications. This is likely to be due to kinematic uncertainty of finger behavior, after encountering unknown objects in arbitrary poses. The authors of [23] determined contact with an underactuated grasper using motor current models. Grasp force regulation and some object shape distinction was achieved in [24] using tactile sensors and closed loop control. The use of tactile contact sensing to further enhance grasping performance through individual finger control was proposed in [21]. In [25], tactile sensing of finger contacts with an object during workspace exploration led to optimal object/hand positioning prior to grasping. Closer to feature extraction, in [26] underactuated fingers equipped with joint sensors re-constructed the contours of immobile rigid objects based on finger positions, while physically exploring a workspace.

3.3 Tactile Feature Extraction in Robotics

Tactile perception techniques in robotics generally fall into categories of feature extraction and object classification, both of which are explored by the proposed hybrid methodology. The majority of techniques rely on active tactile sensor motion via fully actuated robotic systems with full state (i.e., joint angle) feedback. Such approaches have aimed to expose object parameters such as texture [6], [27], stiffness [4], [7], [28], surface contours [2], [26], [29], [30] and thermal properties [7]. In some cases, a direct subset of human inspired exploratory procedures were implemented [3], [6], [7]. In [31], a series of non-human EPs were executed with a parallel jaw gripper to improve force regulation during manipulation. In [6], human inspired EPs facilitated information gathering from a BioTac sensor mounted on an anthropomorphic robot finger. Limited motor resolution of that finger hindered textural/vibration sensing, compared to precision positioning platforms. Four EPs were implemented in early work by Dario et al. [7]. A series of six EPs (variations of pushing and sliding) permitted attribution to 34 'haptic adjectives' [3], interpreted by a classifier.

Though EPs permit significant extension of the spatial and dynamic range of tactile sensors, the procedures are often associated with significant time overheads. The six motions in [3] take over 85 seconds, while the reduced motions of [31] lead to a 30 second grasping process. For industrial processes, this time demand seems excessive.

3.4 Robotic Tactile Classification

Tactile data is often vast, interconnected and noisy. Machine learning approaches have been used to relate such complex data to object class. Following a training process, such systems aim to identify objects from new data. Machine learning approaches have been used both for high-level object class distinction in addition to classifying specific feature properties. In [32] pressure data acquired from gripping vegetables facilitated categorization into three classes of ripeness. Unfortunately, the gripping method destroyed the vegetables, via the combination of open loop control with a fully actuated gripper. In [30], a classifier determined local surface features (edge, face, empty space) in order to construct an overall spatial object model. Active sliding of a six-axis force/torque sensor generated data for neural network based classification into various materials in [33]. The popular vision based object recognition technique 'bag-of-features' was applied to tactile data in [34]. This method constructed a 'vocabulary' of tactile images based on a several grasp locations. Tactile array 'images' gathered during object squeezing and releasing were used as the basis of a *k nearest neighbors'* classifier in [35], though only slight object pose variations were implemented. Unsupervised learning techniques have also been applied to this problem space. Incremental online learning was applied to tactile and joint sensor data in [36] to improve classifier performance. In [37] a sequence of five squeezing actions followed by releasing of an object led to spatial and temporal data for a variety of hands. An unsupervised hierarchical learning methodology was employed and a 1-versus-all classifier obtained.

Reinforcement learning techniques were utilized in [6] to cluster *BioTac* data resulting from exploratory finger motion in order to report stiffness, texture and thermal properties of objects. The work of Chu et al. [3] classified data resulting from 6 EPs into adjectives via machine learning approaches. Classification of the fullness of plastic bottles was achieved in [28] based on a single grasp. Unlike our approach, the bottles had consistent size and orientation, with closed loop force and velocity control of the robot gripper employed to achieve 'safe' container grasping with a PR2 parallel gripper. Such concerns are avoided in our setup via the compliant adaptive gripper. Note that approaches such as [3], [35] only permit object classification once an object has been released. Presumably, any subsequent actions related to object classification (e.g., sorting) would then require re-grasping.

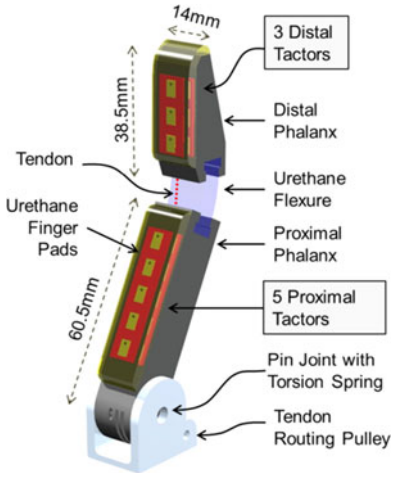

Fig. 4. An underactuated prototype Reflex Hand finger, equipped with barometric TakkTile sensors. There are no position sensors.

The review of existing work has demonstrated trends in tactile identification that favor dense sensory data and extended exploration of objects. It has also been illustrated that though humans make use of EPs, useful haptic object knowledge is also often extracted via minimal, non-exploratory, active haptic interaction [8], [16]. In this work we strive for an equivalent robotic approach based on such minimal interaction. By negating overheads of motion, processing, hardware and time, we propose a solution that is practically implementable. Added to this, we distinguish ourselves from previous work via the robustness of the system to perturbations in object pose (position and orientation) within the grasp of the hand.

4 Experimental Setup

The details of our experimental setup, including the specifics of the underactuated hand and the tactile sensors embedded in the fingers, are explained in this section. The properties of the object used in the experiments are also described.

4.1 Underactuated Robot Hand

The robot hand used in this study (Fig. 1) consists of two prototype fingers of the *Reflex Hand* (manufactured by *Right Hand Robotics, Boston, USA*) mounted on a modified *model T42* base of the Yale OpenHand project [9]. Each *Reflex Hand* finger (Fig. 4) consists of two phalanges with a distal urethane flexure joint and a proximal pin joint with torsional spring. The benefits of this arrangement are described in [9]. Each finger is actuated by a single tendon, attached to a

Fig. 5. The three sets of objects used in this work. Product logos have been obscured for copyright considerations.

Dynamixel MX-28 actuator via a pulley. Unlike in other models of the Reflex Hand, the fingers used in this work (like similar open source designs [9], [10]) do not feature joint position sensing.

4.2 Tactile Sensors

A row of barometric TakkTile force sensors [12] are embedded in the compliant, high-friction grip pads of each link of the robot finger. The grip pads are cast from *'VytaFlex 40'* from *Smooth-On Inc*. The robust and inexpensive ($150 for five sensors) TakkTile sensors are based on urethane encased MEMS barometers, mounted on a PCB with an 8 mm separation. Each finger features eight sensors mounted on two such strips; three sensors on the distal phalanx and five on the proximal phalanx. Each sensor outputs a single pressure value at 100 Hz, with resolution of <0.01 N [12]. The embedded tactile sensors were calibrated using a series of weights (10 to 110 g), illustrating linear responses. This allowed linear sensor equalization (note that calibrated sensor values are only necessary for the parametric methods; the classification method uses uncalibrated values). Sensor 3 of the left finger showed significantly reduced sensitivity and was negated from the parametric processes. Note that the sensor outputs were used only for object classification and parametric estimation and did not provide any type of feedback to the open-loop actuator control scheme.

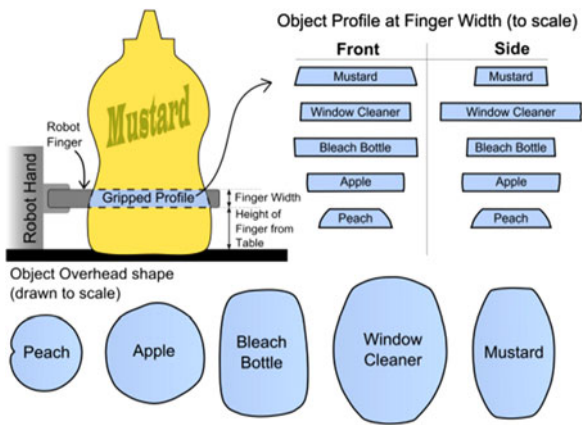

Fig. 6. Side and overhead profiles of 'irregular' everyday objects.

TABLE 1
Sizes (mm) of Model Set 1 Objects

Objects	Small	Medium	Large
Cylinders	50	70	90
Rectangles	50	70	90

4.3 Objects

The experiments were conducted with two sets of 'model objects' and a set of 'everyday' (i.e., household) objects (Fig. 5). The model objects were custom fabricated to constrain parameter variation and validate the parametric estimation methods. The everyday objects were selected from the *YCB object set* [38] to represent a diverse range of size, shape, stiffness and weight parameters. The set is a recent benchmarking standard for robotic manipulation that facilitates replication of test equipment and procedures between research groups. The model objects consisted of two sets, each of which contained circular and cubic objects. The first set were fabricated from 3D printed ABS (wall thickness 4 mm) to maintain stiffness with variations in size. The second set maintained the same size but varied stiffness, via various foam materials. The everyday objects were not constrained by shape, size, or stiffness. Indeed, five out of the 11 objects have irregular and varied shapes and profiles, as illustrated in Fig. 6. Characteristics of the model and everyday object sets are presented in Tables 1, 2 and 3.

Stiffness in all cases was non-destructively measured via a *Transducer Techniques LPO-500* load cell (10 mN accuracy) mounted on a *Robotzone HDA4-50* linear actuator equipped with a *Novotechnik TX2 LVDT* for accurate displacement measurement (0.01 mm resolution). The load cell was placed against the secured object's surface and then extended by 1 to 5 mm, depending on object properties (e.g., a 5 mm compression of the plastic fruit would break it). Change in load cell output was combined with displacement to give a measure of stiffness.

Though the equipment and protocol may introduce some measurement error for stiffer objects, these measurements are only used for validation against stiffness classes and/or a non-linear stiffness scale. As such, coarse stiffness levels are sufficient for our current goals.

5 Methods

In this section we present the details of the machine learning and parametric method algorithms.

5.1 Data Collection

Data was collected by grasping each object with the robot hand 20 times, in various positions and planar orientations, within the workspace of the gripper. An additional seven empty grasps (with no object present) were also recorded.

TABLE 2
Stiffness (N/M) of Model Set 2 Objects

Objects	*Softest (Green)*	*Soft (White)*	*hard (Black)*	*Hardest (Yellow)*
Cylinders	156	346	2,182	97,286
Rectangles	156	346	2,182	51,111

TABLE 3
Characteristics of the Everyday Objects

Objects	Dimensions (mm)	Stiffness side 1 (kN/m)	Stiffness side 2 (kN/m)
Coffee Can	102 × 139	67.2	N/A
Soup can	66 × 101	49.4	N/A
Sugar Box	38 × 89 × 175	4.73	26.87
Apple (plastic)	75	10.6	N/A
Peach (plastic)	59	8.79	N/A
Windex Bottle	80 × 105 × 270	9.87	5.0
Mustard Bottle	80 × 85 × 175	4.69	2.98
Cracker Box	60 × 160 × 230	2.6	3.0
Bleach Bottle	50 × 93 × 250	3.2	3.2
Gelatin Box	28 × 85 × 73	3.1	4.7
Cracker Box	60 × 160 × 230	2.6	3.0

For the everyday objects, 20 grasps were recorded for each object in constrained orientations (±45 degree) and unconstrained orientations (±180 degree). As our method currently involves no post-grasp manipulation (e.g., lifting) the hand was mounted (via clamps) to a table. During each trial (grasp), the actuators were commanded in each case to move 270 degree over 3.25 seconds with a constant target velocity and no influence from sensor feedback (open loop control). The final target position was maintained for 250 ms at the end of the motion before the actuators returned to 0 degree, releasing the object. Actuator target and actual positions, plus force sensor data were recorded at 100 Hz. Images from an overhead webcam were also logged for validation purposes. All logging and control was performed via ROS.

Example of object pose variation is illustrated in Fig. 7, from logged webcam data. Note that the same object surface rested on the table in all cases and that objects were not constrained after placement. It was observed that objects placed in a pose with a horizontal offset would be 'pushed' into the center of the hand by the fingers during grasping (case 1 in Fig. 7). An example of the actuator and force data resulting from a single grasp is demonstrated in the first three plots of Fig. 8. Other features of this figure will be further described in subsequent sections.

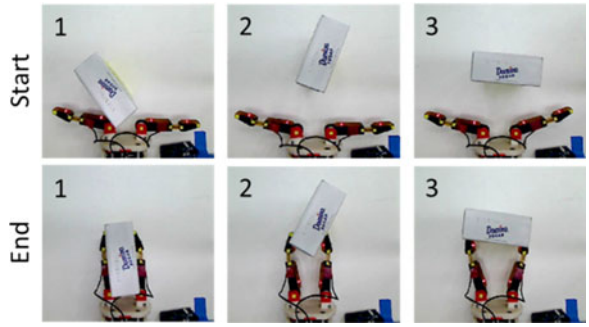

Fig. 7. Examples of object pose variation and resulting grasp.

5.2 Machine Learning Scheme

In this subsection we present the machine learning scheme, which aims to identify objects from the data acquired during a single grasp. A classifier based on the random forests technique was employed.

5.2.1 *Random Forests Classifier*

Random forestswere originally proposed by Ho [39] and Breiman [40] and are an ensemble classifier based on different decision trees. The output is the most popular class between the decisions of the individual classifiers. The RF technique provides high classification accuracy and handles multiclass problems, such as distinguishing between multiple objects with different properties. Furthermore, the method is fast and efficient when dealing with large databases and has the

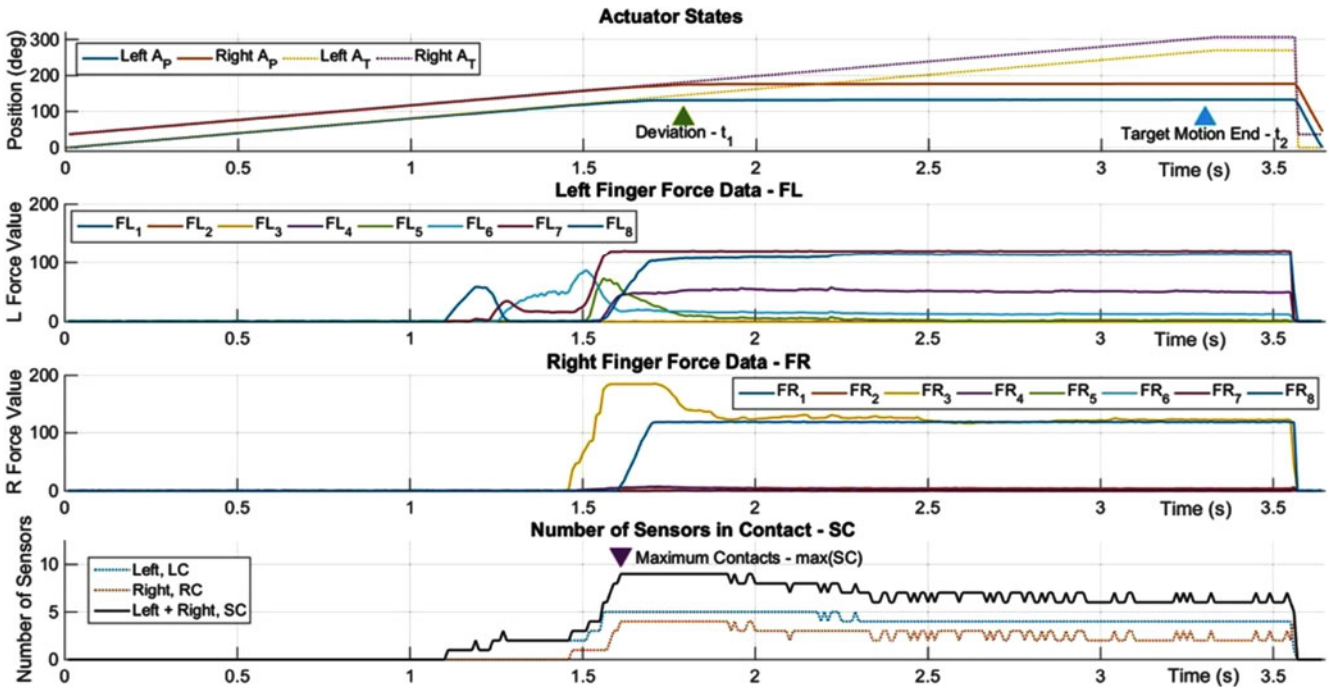

Fig. 8. Actuator position and force sensor data during a single object grasp. Triangular markers denote events identified by the methodology. The bottom plot shows the number of sensors in contact during a grasp. The stable grasp start may occur before or after actuator deviation.

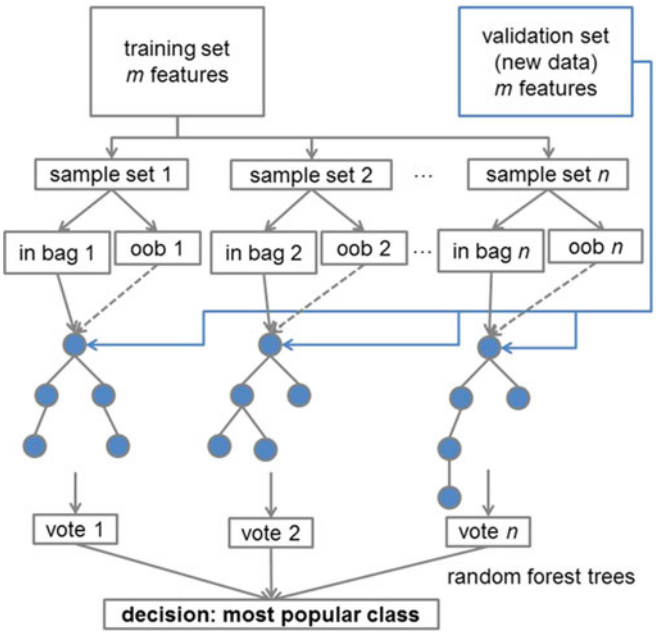

Fig. 9. The random forests classifier constructed with n trees.

capability to handle high numbers of input variables. A diagram of the RF classification procedure for n trees is presented in Fig. 9. Each tree of the RF is constructed from a different out-of-bag (*oob)* sample set from the training data. This training data comprises two thirds of the recorded grasps data. The remaining data is used for validation. Comparison of RF technique to various state-of-the-art classifiers, will be presented as part of the results (Section 6.1.1).

5.2.2 Feature Selection

The feature space used for discriminating between the objects is defined by the actuator and force sensor data at two different time instances of the grasping process (an additional third time instance is sampled by the parametric method). The first instance (t_1) is taken when the sum of actuator target positions (A_T) exceeds the sum of actual actuator positions (A_P) by a given threshold, ($T_{Stall} = 20$ deg) via $|A_T - A_P| > T_{Stall}$. This deviation indicates a stall in actuator motion due to finger /object interaction. The second instance (t_2) occurs when actuator target positions (A_T) have reached the steady state ($t = 3.25$ s) at which time hand reconfiguration has stopped and the system is at an elastic equilibrium. Here, the object is being held with constant tendon exertion. These instances are indicated as 'Deviation' and 'Target Motion End' on Fig. 8. Actual actuator positions (two values) and force sensor readings (16 values) are extracted at these two instances, giving a feature space of 36 variables. This raw data is obtained without a-priori information regarding the robot model or actual joint angles, making the machine learning methodology model-free. Another beneficial characteristic of the classifier is that it does not require calibrated force values, as classification is based on the differentiation in input data.

5.2.3 Feature Importance Calculation

The RF technique has an inherent capability of computing the importance scores for all feature variables and comparing them. Such a calculation is useful for optimizing the hand designs, by minimizing the number of sensors required to achieve a certain level of classification accuracy. When fewer sensors are used, their locations on the fingers become more critical.

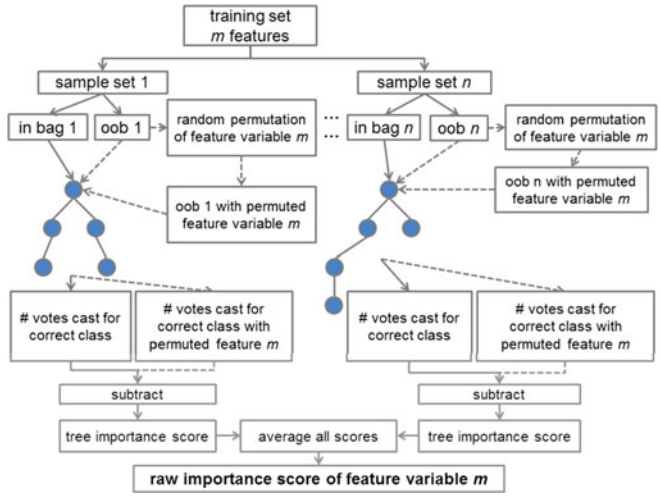

Fig. 10. Random forests feature importance calculation.

Importance calculation is based on manipulations of a subset of the training data, which are called out-of-bag (*oob*) samples. These *oob* samples are given as an input to all decision trees and the numbers of correct votes are counted. Then, the *oob* samples values of a feature variable m are randomly permuted. The modified samples are once again "fed" to each of the n decision trees. Importance of the feature variable m is then calculated by the operation $I_m = V_P - V_U$. Where Vp is the number of correct votes cast with the m-variable permuted *oob* data and V_U is the same metric with the untouched *oob* data.

The overall/raw importance score (I_m) for each feature variable m, is the average of the importance scores computed for all trees of the RF. The process is described in Fig. 10. In this work, we normalize importance scores to facilitate comparisons of the different feature variables, even for different classification problems.

5.3 Parametric Method

The parametric method estimates physical object parameters of size and stiffness based on data acquired during the grasp. Size is related to a contact polygon constructed from force and actuator data. A measure of grasp stability is also provided. The parametric method makes use of several processes, as illustrated in Fig. 11.

5.3.1 Forward Kinematics Estimator

To estimate the size and shape of an object, the parametric method relies on knowledge of the kinematic position of the robot fingers once a secure grasp has been made. Predicting the kinematic behavior of mechanically compliant underactuated fingers is non-trivial. In addition to the complexities of modelling flexure joints [41], multiple joint position solutions exist for each actuator position. Actual finger kinematics result from finger and transmission dynamics, which are modulated during different stages of an adaptive grasp by interaction with unknown objects [20]. In the case of the

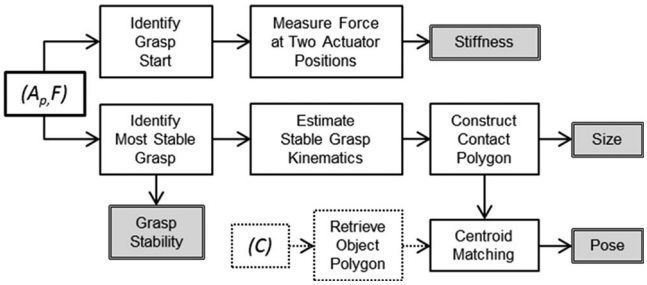

Fig. 11. Processes within the parametric estimator. Outputs are shaded boxes. Classifier dependent components (such as object class, C) have dotted lines.

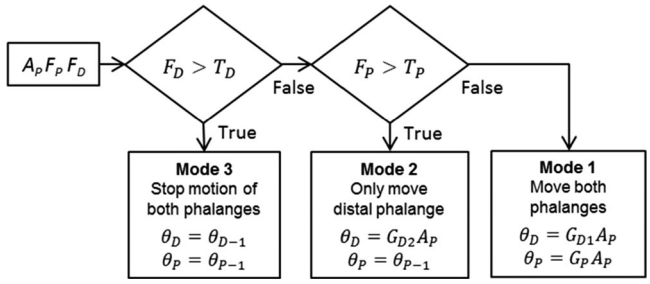

Fig. 12. Kinematic estimation via actuator positions (AP) with proximal (FP) and distal (FD) force sensor values.

fingers used in this work, the inclusion of tactile sensors permits contact detection on each phalange. Based on this, a computationally efficient kinematics estimator (Fig. 12) was constructed that uses force sensor data to switch between different grasping 'modes' (Fig. 13). In each mode, a different set of transmission gains (G_{D1}, G_{D2}, G_P) converts actuator position (A_P) to motion of the proximal and distal joint (θ_P, θ_D). A_P is also equivalent to tendon length from fingertip anchor to actuator. For simplicity, θ_D is considered as a pin joint in the kinematic structure of the finger. Mode selection is based on F_P and F_D, which are the sum of individual force sensor values on the proximal and distal phalanges respectively. The force value thresholds required to halt the motion of each joint are defined independently as T_D and T_P. These values were determined experimentally and are higher than the threshold used for contact detection, T_C. This allows the method to deal with the common case of a single finger pushing an object into the center of the hand (e.g., case 1 of Fig. 7), prior to a grasp being made. The different modes may be explained as follows:

- *Mode 1 - Pre-contact*: 'Free motion' of the finger prior to object contact. Actuator motion generates a large change in θ_P and small change in θ_D.
- *Mode 2 – Proximal Contact*: If $F_P > T_P$ motion of the θ_P stops. Actuator motion is transferred to θ_D.
- *Mode 3 – Proximal & Distal Contact*: If $F_D > T_D$ motion of both joints stop.
- *Mode 3a – Distal Only Contact*: Mode 3a in Fig. 13 denotes a distal only grasp (no proximal contact).
- This is also recognized by $F_D > T_D$ (same as Mode 3) but without precedence by a proximal contact.

The forward kinematics method is iterative and as such, determination of joint angles for a specific instance necessitates calculation of all joint angles up until that instance. Due to a lack of typical kinematic matrix operations, this process has very little computational overhead. Kinematics estimation for all of the 3,250 time intervals involved in a complete grasp (e.g., the data shown in Fig. 8) takes less than 30 ms using Matlab on an Intel i7 3.6 Ghz PC. Motion gains and threshold values were determined via a calibration process in which joint angles were visually observed from ten overhead video frames recorded during an empty grasp and a grasp of a rigid 70 mm cylinder. Joint angles were determined by locating the spatial centroid of small visible markers attached to the finger phalanges. These markers are visible in Figs. 7 and 14. Interpolation of marker co-ordinates with synchronized actuator data led to linear transmission models and three gains. These gains (for left and right fingers) are proximal $G_P = (3.58, 3.38)$, distal during mode 1 $G_{D1} = (0.26, 0.11)$ and distal during mode 2 $G_{D2} = (5.29, 5.06)$. Re-orientating the hand with respect to gravity can modify these gains. When the hand is orientated in the direction of gravity, as opposed to the lateral case of our experimental setup, the proximal joints displace approximately 1 degree more for 90 degree of actuator rotation. It is likely that gain interpolation from several discrete observations would permit kinematic estimation for a range of hand orientations.

5.3.2 Grasp Type, Location, and Quality

The hand kinematics may be combined with force data to establish the spatial co-ordinates of contact points on the finger pads for any instance of grasp data. A suitable instance for further object analysis is the moment when maximum stability has been achieved for a grasp. In this

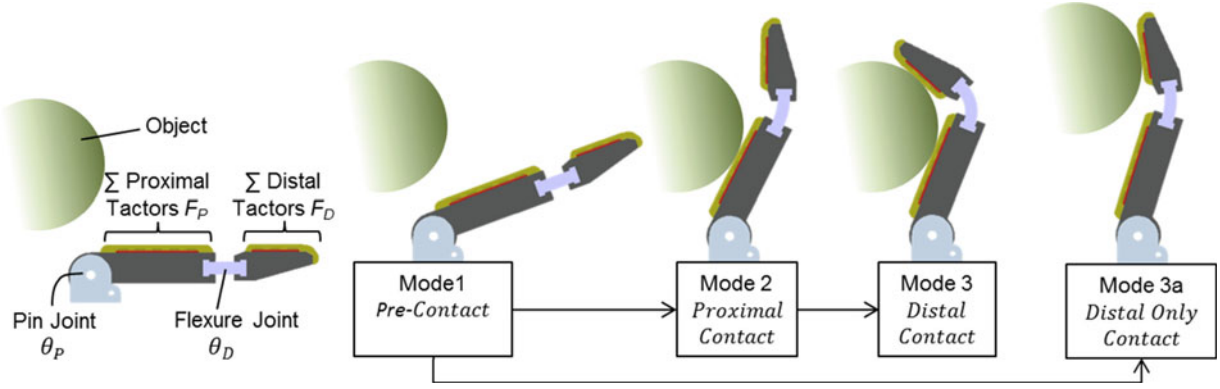

Fig. 13. Kinematic mode progression based on finger adaptation to object contact.

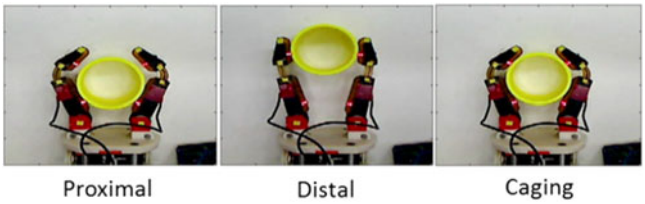

Fig. 14. Examples of the three grasp types.

work we associate grasp stability with the number of contacts of the hand with the object, which is also suggested in [42]. Prior to this moment, the object is more likely to move within the grasp. Afterwards, the object may be compressed and deformed. Counting the number of sensors whose values exceed a given contact threshold (T_C) at each time instance (t) of the grasp produces the following 'sensors-in-contact' array $SC(t)$

$$SC(t) = \sum_{i=1}^{n=8} LC_i(t) + \sum_{i=1}^{n=8} RC_i(t) \tag{1}$$

$$where\ LC_i = \begin{cases} 1, & FL_i > T_C \\ 0, & FL_i \leq T_C, \end{cases} \quad RC_i = \begin{cases} 1, & FR_i > T_C \\ 0, & FR_i \leq T_C. \end{cases} \tag{2}$$

Where LC and RC are a binary array of the sensors in contact, derived from the force values FL and FR. FL and FR are force sensors measurements on left and right fingers. The SC array is searched to locate the first instance of $max(SC)$, the maximum sensors in contact. This instance is indicated on Fig. 8 as 'Maximum Contacts'. The process is highly efficient and may be computed at t_2 with no requirement to release the grasp.

The value of $max(SC)$ may be used to give an indication of grasp stability (G_S), when combined with grasp type determination (proximal, distal or caging, as illustrated in Fig. 13). Grasp type is determined by counting the number of proximal (C_D) and distal (C_P) contacts

$$C_P = \sum_{i=1}^{n=5} LC_i(t) + RC_i(t), C_D = \sum_{i=6}^{n=8} LC_i(t) + RC_i(t). \tag{3}$$

Each grasp type is represented by a gain (G_T) associated with the stability of that grasp. The number of sensors in contact SC, is scaled by G_T to give the G_S score

$$G_S = G_T SC(t),\ where\ G_T = \begin{cases} 1, & C_P = 0 \wedge C_D > 0 \\ 1.2, & C_P > 0 \wedge C_D = 0 \\ 2, & C_P > 0 \wedge C_D > 0. \end{cases} \tag{4}$$

The highest gain (2) is associated with a caging grasp, where the object is secured by both proximal and distal links. The proximal only grasp is rated slightly higher (1.2) than a distal only grasp (1), due to a tendency for an object that slips from a distal grasp to become secured by a proximal grasp. These gains have been determined subjectively based on observations from a variety of underactuated robot hands when interacting with the extended YCB object set [38]. Example G_S scores will be provided for different example cases in Section 6.2.1.

5.3.3 Grasp Polygon Construction

The kinematics estimator also permits the location of contact points to be established at $\max(SC)$. At this point, the co-ordinates of in-contact sensors may be determined from finger kinematics (Section 5.3.1) and the arrays LC and RC. These co-ordinates construct convex *grasp polygons*, as will be later presented Section 6.2.1 and Fig. 18.

The grasp polygon provides spatial aspects of the object and grasp. One easily extractable feature is the grasp aperture (polygon width), which may be used as a simple dimensional output. We use this metric for verification of the classifier results (further detailed in Section 6.3.1).

5.3.4 Stiffness Estimation

Estimation of object stiffness is achieved by observing the change in all measured forces between two intervals in the grasp. Due to the limits of available data, it is not possible to fulfill the stiffness equation $S = \Delta F/\Delta x$, where stiffness, S, is measured by observing a change in force ΔF for a change in surface displacement Δx. This is because the change in finger position after a grasp has been established cannot be accurately measured. However, we have found that a metric related to object stiffness (S_M) may be achieved by considering the average reaction force per tactile sensor at two instances of the grasping process. These intervals are the same as those used for feature selection (defined in Section 5.2.2), i.e., the actuator stall instance (t_1) and the steady state condition of $A_T(t_2)$. This capability results from the open-loop nature of the grasp, which maintains some consistency between conditions

$$F(t) = \sum_{i=1}^{n=8} LC_i(t)FL_i(t) + RC_i(t)FR_i(t), \tag{5}$$

$$S_M(t) = \frac{|F(t_1)|}{SC(t_1)} + \frac{|F(t_2)|}{SC(t_2)}. \tag{6}$$

Where LC, RC and SC were defined in equations (1) and (2). By combining (FL, FR) with (LC, RC), the values of non-contacting sensors are set to zero, reducing noise. Other methods of stiffness estimation that incorporate differences in actuator position error and time were evaluated, but led to large error margins with variations in grasp type and pose, particularly for stiffer objects. Stiffness estimation of object set 2 is presented in Section 6.2.2.

5.3.5 Pose Estimation

Pose estimation allows the location of objects within a grasp to be estimated based on object class and contact locations. As such, the technique is facilitated by a synergistic collaboration between the machine learning and parametric methods. Pose information is useful for determining subsequent manipulation of an object. For example, placing a grasped object precisely on a target location will require different hand positioning depending on the location of the object in the hand. The pose estimator functions by using the object class (C) to recall a simple polygon model of an object's cross section, based on size and shape. For example, the apple object polygon is a circle 75 mm diameter. The centroid of the object polygon is matched to the Y

TABLE 4
Classification Results for All Experiments

Objects	Case	Accuracy
Model 1	Size & Shape	93.57%(SD: 3.25%)
Model 2	Shape & Stiffness	93.01%(SD: 3.02%)
Everyday	Constrained Orientations	100% (SD: 0%)
Everyday	Free Orientations	94.32%(SD: 3.09%)

(distal) component of the centroid of the grasp polygon to align actual and recalled data. Currently this method functions only for circular objects, as non-round objects have multiple solutions.

6 Results

6.1 Classification Results

For the training of the random forest classifiers, a 10-fold cross-validation procedure [43] was used to assess efficiency and avoid overfitting. The classification accuracies are reported in Table 4.

These results were computed by averaging multiple rounds of the cross-validation method. For all objects, data from 12 of the acquired 20 grasps were used for training, with the remaining eight grasps used for validation. Discussion of these results follows.

6.1.1 Comparison of Various Classifiers

To test the suitability of the RF machine learning approach to this problem, the classification of everyday objects in constrained orientations was repeated with a number of alternative state-of-the-art classifiers. The methods used were a Linear Discriminant Analysis (LDA), a Naïve Bayes classifier, a Neural Network (NN), a binary Support Vector Machines classifier (SVM) and the Random Forests technique. The SVM classifier was trained using different kernels (linear, RBF etc.) and the best results were acquired. The NN classifier was constructed using a single hidden layer with fifteen hidden units trained with the Levenberg-Marquardt back-propagation algorithm. RF forests were grown with ten trees for processing speed (two times faster) and one hundred trees for accuracy. All classifiers were compared for the task of discriminating between the everyday objects with constrained orientations (±45 degree) and arbitrary positions. The classification accuracies for the different techniques are reported in Table 5. Random forests outperform all other classification methods, but all methods provide high classification accuracies.

TABLE 5
Comparison of Different Classifier Accuracy on Everyday Objects with Constrained Orientations

Classifier	Classification Accuracy
LDA	89.74%
NB	90.41%
NN	95.65%
SVM	92.30%
RF (10 trees)	98.04%
RF (100 trees)	100%

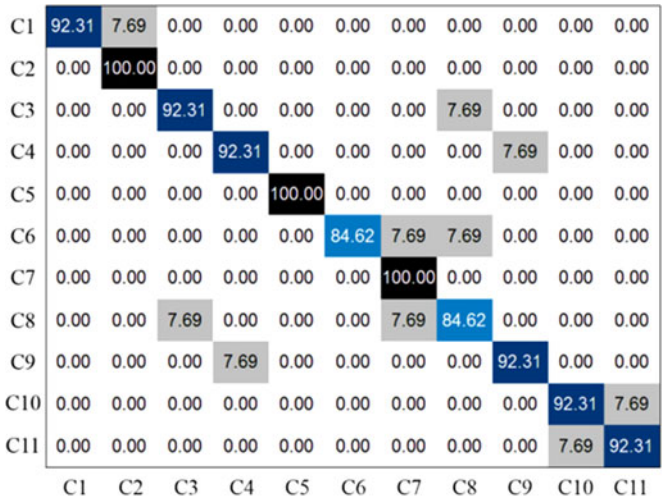

Fig. 15. Confusion matrix for the case of classifying everyday objects with unconstrained orientations.

6.1.2 Model Objects Classification Results

The first classification problem involved discrimination between the model objects of set 1 and 2 (see Section 4.3). The trained classifier is slightly better at discriminating between objects with different shapes and sizes rather than objects of different shapes and stiffness. Classification results for this problem are presented in Table 4.

6.1.3 Everyday Objects Classification Results

The second classification problem involved discrimination between the various everyday objects. Two cases are analyzed; constrained orientation and free orientation (as described in Section 5.1). As expected the classification accuracy is higher for the constrained orientations case, though the free orientation result also demonstrates excellent accuracy. Results are presented in Table 4.

In Fig. 15 we present a confusion matrix for the case of classifying everyday objects with unconstrained orientations. The diagonal elements represent the correctly classified trials while the non-diagonal elements represent the misclassifications. It may be noticed that the classifier is very efficient in discriminating between the examined objects, with only a few objects appearing harder to distinguish (apples may be classified as apricots, the gelatin box may be identified as the sugar box, the bleach is sometimes confused with the Windex etc.). These misclassifications are caused by dimensional similarities between certain sides of dissimilar objects.

6.1.4 Sensor Placement Optimization

Feature variable importance was implemented to determine optimal force sensor locations for different quantities of force sensors. The feature variables importance scores for all 36 features (18 features at two time instances—Section 5.2.2) are presented in Fig. 16, for the cases of everyday objects with constrained and free orientations. The height of the bars represents the importance scores of the features for 10 sets (a distinct random splitting of the training data). All scores are shown to be robust along all sets. To evaluate this approach, the most important feature variables were selected

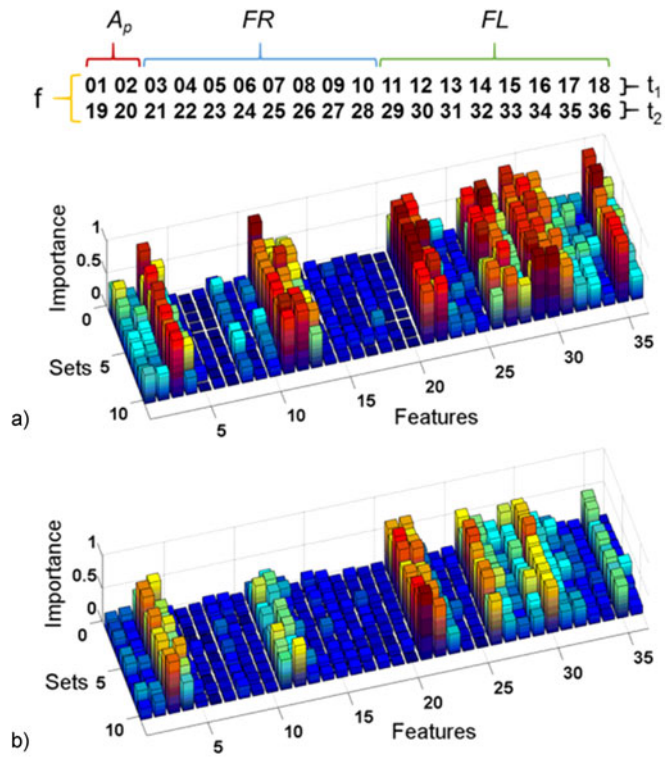

Fig. 16. Feature variables importance bar plots for discrimination of everyday objects with a) constrained and b) free orientations.

and the classifier was re-trained after removal of the redundant features. Three different cases were examined, performing retraining for the four, six and eight most 'important' sensors of the hand (shown in Fig. 17), based on these values, rather than using the initial 16 sensors. Table 6 reports classification results for all cases.

These results illustrate a significant redundancy in the initial feature space, with respect to classification method. In this respect, future hands could be constructed with fewer sensors based on the generated designs (Fig. 17). In all cases the designs indicate a preference for sensor placement on the proximal regions of the phalanxes. The asymmetrical nature of the results is likely to be due to sensitivity of particular tactors and/or tendon tension difference between the robot fingers.

6.2 Parametric Method Results

Parametric results of dimension, stiffness and in-grasp pose estimation will now be presented.

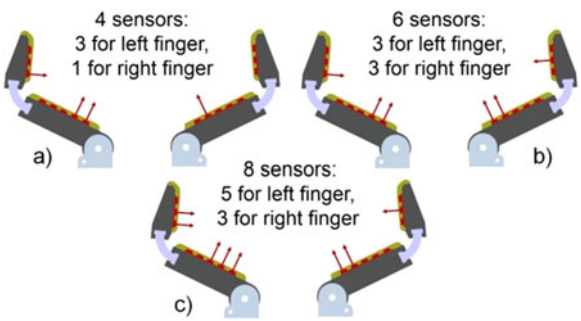

Fig. 17. Optimal sensor placement for six and eight sensor setups based on features variables importance.

TABLE 6
Effect of Sensor Reduction on Classification Accuracy for Everyday Objects

Sensors	16 (All)	8	6	4
Accuracy	94.32%	95.78%	93.14%	94.67%
SD	3.09%	3.7%	2.67%	3.79%

6.2.1 Dimension Estimation

Dimension estimation was performed for the 50, 70 and 90 mm diameter cylindrical model objects of set 1 (Fig. 5) with unconstrained starting positions. Dimensions were based on grasp polygon width, derived from the estimated finger kinematics. Examples of determined grasp polygons for an everyday object (box of sugar) are shown in Fig. 18. These examples also show the measure of grasp stability G_S, as defined in Section 5.3.2. Fig. 18 illustrates some kinematic mismatch, which is largely due to simplistic modelling of the urethane flexure joint as a pin joint (thus ignoring dynamic properties and out-of-plane motion), in addition to occasional variation in contact detection. This impacts the accuracy of kinematic mode-selection (Fig. 13).

Fig. 19 provides a histogram of estimated dimensions for all grasps. Clear distinctions are illustrated between the different objects sizes, following a trend consistent with the actual diameters of the objects, though a linearly increasing offset between estimated and actual values may be observed. It may be seen that sizable error bounds are present, particularly for the smaller, 50 mm diameter cylinder. Grouping the dimension estimations by grasp types in Fig. 20 illustrates persistent errors for the 50 mm object with the caging grasp. Conversely, little variance is indicated overall for proximal grasps. The results reflect the possibility that kinematics estimator accuracy is dependent on the grasp type. Indeed, a distal grasp can lead to further object motion (e.g., pulling the object towards the palm). Of course, the grasp does not always occur at the widest point of the object, leading to a negative offset in some cases.

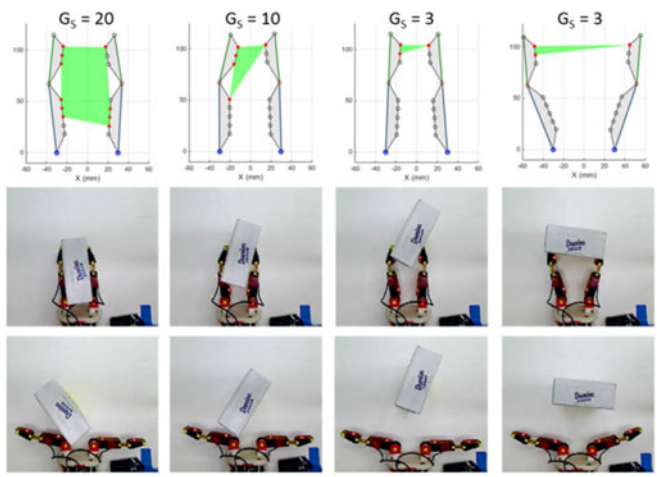

Fig. 18. Top row: grasp polygon reconstruction from finger kinematics estimation. G_S shows grasp stability score. Middle row: corresponding video frame of the most stable grasp instance, based on *max(SC)*. Bottom row: object starting pose.

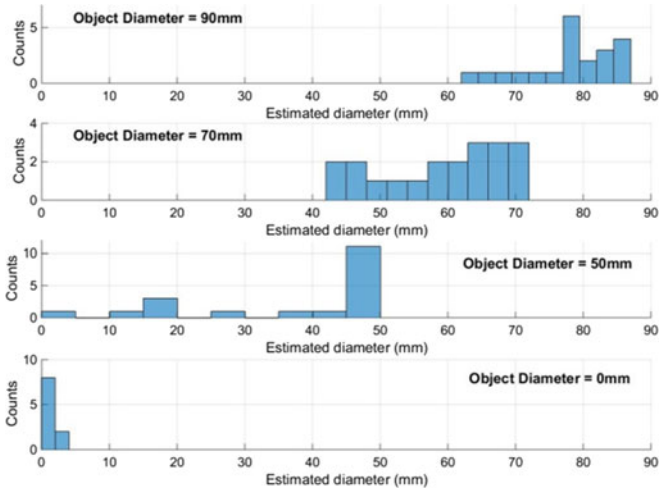

Fig. 19. Histogram of parametrically estimated diameters of three stiff cylinder objects (from model set 1) and an empty grasp.

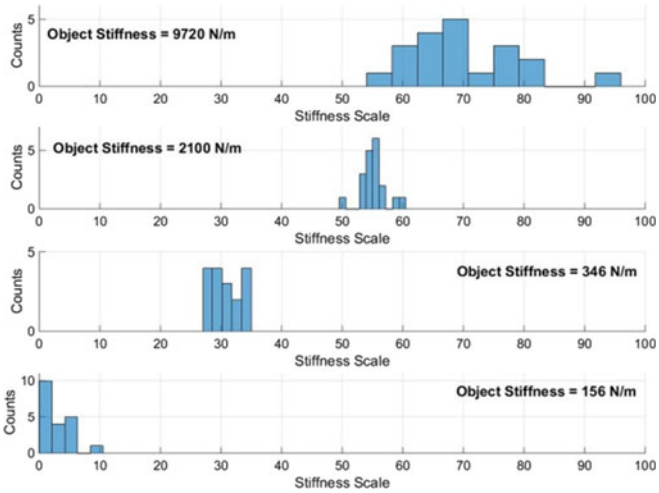

Fig. 21. Histogram of parametrically estimated stiffness (scale 0-100) with for various stiffness cylinders (from model set 2).

6.2.2 *Stiffness Estimation*

Parametric stiffness estimations for set 2 of the model objects (Fig. 5) are illustrated in Fig. 21. The outputs of the stiffness metric S_M were scaled between values of 0-100. The results indicate excellent distinction between three different stiffness objects (in the range 156 to 2100 N/m) with some larger distribution of errors for the most rigid object (where sensor output would often saturate during the grasp). Inspection of S_M distribution in Fig. 22 illustrates that the results do not overlap within each grasp type. Therefore, by determining the grasp type G_S via equation (4), it is possible to automatically categorize each result into an appropriate stiffness value.

6.3 Collaborative Results

The following brief results are based on collaboration (data sharing) between the parametric method and classifier to improve performance and extract further data.

6.3.1 *On-Line Classifier Retraining*

Dynamic classifier retraining uses the dimension estimated by the parametric method to improve classifier performance. By omitting objects whose dimensions are inconsistent with the measured parameter it is possible to validate the initial classifier decision and, if necessary, reject the decision and re-train the classifier with a new, dynamically reduced data set.

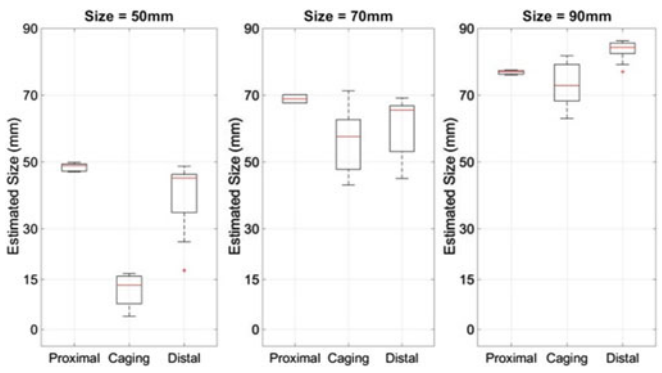

Fig. 20. Stiff cylinders diameter estimation, grouped by grasp type.

As a hypothetical example, say the classifier were to mistakenly classify a soup can as a coffee can, perhaps due to an extreme object starting position. The estimated object dimension (provided by parametric method) immediately indicates that the grasped object is too small to be a coffee can, given known dimensions from Table 3. The classification decision is therefore verified as false, and the classifier is dynamically retrained, excluding all the objects from the training set whose dimensions are significantly different from the estimated dimension. Essentially, this is an a-posteriori filtering and correction of the classification decisions that increases the machine learning approach's efficiency. The retraining and reclassification (which takes less than 65 ms) may be completed without re-grasping the object. The approach was tested on the failed cases of unconstrained everyday object presented in Table 4. In all cases, dynamic re-training led to correct identification of the object class.

6.3.2 *Pose Estimation*

Collaboration also occurs by passing the classifier output to the parametric method (as in Section 5.3.5). This enables estimation of pose for round (orientation free) objects. Such pose estimation can be useful for accurate placement of objects after grasping, e.g., for multiple part assembly or the placement of an item into packaging. Sample results of this approach are illustrated in Fig. 23 for proximal, distal and

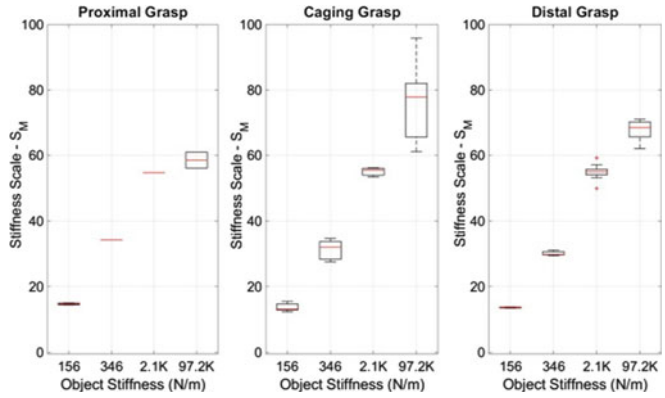

Fig. 22. Stiffness estimation results, grouped by grasp type.

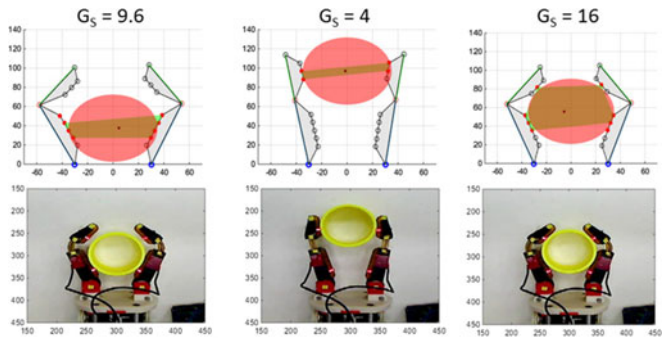

Fig. 23. Pose estimation of a cylinder. The object class polygon (circle) overlaps the contact polygon. G_S scores are provided.

caging grasps of a 70 mm rigid cylinder. Accurate kinematic estimation of finger pose is also shown in Fig. 23. The geometric cylinder model was loaded into the parametric approach via the object class.

7 Conclusion

In this paper we have presented a hybrid methodology for performing tactile classification and feature extraction during a single grasp with a simple underactuated robot hand. Such hands constitute easily implementable practical robotic grasping solutions. Similarly, our work has aimed to provide a system with low computation and complexity overheads for haptic sensing applications in practical robotics. Despite this, we believe our approach is scalable to other robotic hands with alternative sensing and actuation, providing that adaptive grasping may be implemented. In many cases this may need to be via a motor control, rather than a mechanical approach.

Promising results have been presented, showing high classification accuracy and the ability to extract several object features (object dimension, stiffness and pose) within error bounds. While more accurate parameter identification has been carried out by other robotic approaches, these have tended to focus on a single parameter as part of an extensive tactile exploration process. Though our classification and parametric methods can work independently, a novel collaborative scheme allows outcomes to be combined. This improves classification accuracy and facilitates estimation of object pose. The various aspects of the proposed methodology are highly suited to dynamic, semi-structured environments where the time or hardware necessary for detailed haptic object exploration is not available.

Acknowledgments

The authors would like to thank Raymond R. Ma for his expertise in robot hand design. Kevin Gemmell is acknowledged for assistance in object stiffness measurements. This work has been partially supported by the US National Science Foundation (NSF) NRI grant IIS-1317976.

References

[1] S. J. Lederman and R. L. Klatzky, "Extracting object properties through haptic exploration," *Acta Psychologica*, vol. 84, pp. 29–40, 1993.

[2] A. M. Okamura, M. L. Turner, and M. R. Cutkosky, "Haptic exploration of objects with rolling and sliding," in *Proc. IEEE Int. Conf. Robot. Autom.*, vol. 3, 1997.

[3] V. Chu, I. McMahon, L. Riano, C. G. McDonald, J. M. Perez-Tejada, M. Arrigo, N. Fitter, J. C. Nappo, T. Darrell, and K. J. Kuchenbecker, "Using robotic exploratory procedures to learn the meaning of haptic adjectives," in *Proc. IEEE Int. Conf. Robot. Autom.*, 2013, pp. 3048–3055.

[4] Z. Su, J. A. Fishel, T. Yamamoto, and G. E. Loeb, "Use of tactile feedback to control exploratory movements to characterize object compliance," *Frontiers Neurorob.*, vol. 6, pp. 1–9, 2012.

[5] A. Bierbaum, M. Rambow, T. Asfour, and R. Dillmann, "A potential field approach to dexterous tactile exploration of unknown objects," in *Proc. 8th IEEE-RAS Int. Conf. Humanoid Robots, Humanoids*, 2008, pp. 360–366.

[6] J. A. Fishel and G. E. Loeb, "Bayesian exploration for intelligent identification of textures.," *Frontiers Neurorob.*, vol. 6, p. 4, Jan. 2012.

[7] P. Dario, P. Ferrante, G. Giacalone, L. Livaldi, B. Allotta, G. Buttazzo, and A. M. Sabatini, "Planning and executing tactile exploratory procedures," in *Proc. IEEE/RSJ Int. Conf. Intell. Robots Syst.*, vol. 3, 1992, pp. 1896–1903.

[8] R. L. Klatzky and S. J. Lederman, "Identifying objects from a haptic glance," *Perception Psychophys.*, vol. 57, no. 8, pp. 1111–1123, 1995.

[9] R. R. Ma, L. U. Odhner, and A. M. Dollar, "A modular, open-source 3D printed underactuated hand," in *Proc. IEEE Int. Conf. Rob. Autom.*, 2013, pp. 2737–2743.

[10] L. U. Odhner and A. M. Dollar, "Stable, open-loop precision manipulation with underactuated hands," *Int. J. Robot. Res.*, vol. 34, no. 11, pp. 1347–1360, 2015.

[11] M. Liarokapis, B. Calli, A. Spiers, and A. Dollar, "Unplanned, model-free, single grasp object classification with underactuated hands and force sensors," in *Proc. IEEE/RSJ Int. Conf. Intell. Robots Syst.*, 2015, pp. 5073–5080.

[12] Y. Tenzer, L. P. Jentoft, and R. D. Howe, "The feel of MEMS barometers: Inexpensive and easily customized tactile array sensors," *IEEE Robot. Autom. Mag.*, vol. 21, no. 3, pp. 89–95, Sep. 2014.

[13] R. S. Johansson and J. R. Flanagan, "Coding and use of tactile signals from the fingertips in object manipulation tasks," *Nat. Rev. Neurosci.*, vol. 10, no. 5, pp. 345–59, May 2009.

[14] S. J. Lederman and R. L. Klatzky, "Hand movements: A window into haptic object recognition," *Cognitive Psychol.*, vol. 19, no. 3, pp. 342–368, Jul. 1987.

[15] N. Wettels, J. A. Fishel, Z. Su, C. H. Lin, and G. E. Loeb, "Multimodal synergistic tactile sensing," in *Proc. IEEE/RAS Int. Conf. Humanoid Robot.*, vol. 105, no. 2, 2009, pp. 2–4.

[16] S. J. Lederman and R. L. Klatzky, "Haptic identification of common objects: Effects of constraining the manual exploration process.," *Perception Psychophys.*, vol. 66, no. 4, pp. 618–628, 2004.

[17] E. B. Vander Poorten, E. Demeester, and P. Lammertse, "Haptic feedback for medical applications, a survey," in *Proc. Actuator*, 2012, pp. 519–525.

[18] A. Spiers, S. Baillie, T. Pipe, and R. Persad, "Experimentally driven design of a palpating gripper with minimally invasive surgery considerations," in *Proc. IEEE Haptics Symp.*, Mar. 2012, pp. 261–266.

[19] R. L. Klatzky, J. M. Loomis, S. J. Lederman, H. Wake, and N. Fujita, "Haptic identification of objects and their depictions," *Perception Psychophys.*, vol. 54, no. 2, pp. 170–178, 1993.

[20] L. Birglen, T. Laliberté, and C. M. Gosselin, "Underactuated robotic hands," in *Springer Tracts in Advanced Robotics*. Berlin, Germany: Springer Science & Business Media, 2008, p. 244.

[21] L. P. Jentoft, Q. Wan, and R. D. Howe, "Limits to compliance and the role of tactile sensing in grasping," in *Proc. IEEE Int. Conf. Robot. Autom.*, May 31, 2014-Jun. 7, 2014, pp. 6394–6399.

[22] A. M. D. Ravi Balasbramanian, "A framework for studying underactuation in the human hand," in *Proc. Annu. Meet. Americal Soc. Biomechanics*, 2010, pp. 5–6.

[23] B. Belzile and L. Birglen, "A compliant self-adaptive gripper with proprioceptive haptic feedback," *Auton. Robots*, vol. 36, pp. 79–91, 2014.

[24] H. Tsutsui, Y. Murashima, N. Honma, and K. Akazawa, "Robot hand with soft tactile sensors and underactuated control," in *Proc. Annu. Int. Conf. IEEE Eng. Med. Biol. Soc.*, 2013, pp. 4148–4151.

[25] A. M. Dollar, L. P. Jentoft, J. H. Gao, and R. D. Howe, "Contact sensing and grasping performance of compliant hands," *Autonomous Robots*, vol. 28, no. 1, pp. 65–75, 2010.

[26] L. P. Jentoft and R. D. Howe, "Determining object geometry with compliance and simple sensors," in *Proc. IEEE/RSJ Int. Conf. Intell. Robots Syst.*, 2011, pp. 3468–3473.

[27] A. Drimus, M. Borlum Petersen, and A. Bilberg, "Object texture recognition by dynamic tactile sensing using active exploration," in *Proc. 21st IEEE Int. Symp. Robot Human Interactive Commun.*, 2012, pp. 277–283.
[28] S. Chitta, M. Piccoli, and J. Sturm, "Tactile object class and internal state recognition for mobile manipulation," in *Proc. IEEE Int. Conf. Robot. Autom.*, 2010, pp. 2342–2348.
[29] A. M. Okamura and M. R. Cutkosky, "Feature detection for haptic exploration with robotic fingers," *Int. J. Robot. Res.*, vol. 20, no.12, pp. 925–938, 2001.
[30] U. Martinez-Hernandez, G. Metta, T. J. Dodd, T. J. Prescott, L. Natale, and N. F. Lepora, "Active contour following to explore object shape with robot touch," in *Proc. World Haptics Conf.*, Apr. 2013, pp. 341–346.
[31] J. M. Romano, K. Hsiao, G. Niemeyer, S. Chitta, and K. J. Kuchenbecker, "Human-inspired robotic grasp control with tactile sensing," *IEEE Trans. Robot.*, vol. 27, no. 6, pp. 1067–1079, Dec. 2011.
[32] I. Bandyopadhyaya, D. Babu, A. Kumar, and J. Roychowdhury, "Tactile sensing based softness classification using machine learning," in *Proc. IEEE Int. Adv. Comput. Conf.*, 2014, pp. 1231–1236.
[33] H. K. Lam, U. Ekong, H. Liu, B. Xiao, H. Araujo, S. H. Ling, and K. Y. Chan, "A study of neural-network-based classifiers for material classification," *Neurocomputing*, vol. 144, pp. 367–377, Nov. 2014.
[34] A. Schneider, J. Sturm, C. Stachniss, M. Reisert, H. Burkhardt, and W. Burgard, "Object identification with tactile sensors using bag-of-features," in *Proc. IEEE/RSJ Int. Conf. Intell. Robots Syst.*, 2009, pp. 243–248.
[35] A. Drimus, G. Kootstra, A. Bilberg, and D. Kragic, "Design of a flexible tactile sensor for classification of rigid and deformable objects," *Robot. Auton. Syst.*, vol. 62, no. 1, pp. 3–15, Jan. 2014.
[36] H. Soh and Y. Demiris, "Incrementally learning objects by touch: Online discriminative and generative models for tactile-based recognition," *IEEE Trans. Haptics*, vol. 7, no. 4, pp. 512–25, Jan. 2014.
[37] M. Madry, L. Bo, D. Kragic, and D. Fox, "ST-HMP: Unsupervised Spatio-Temporal feature learning for tactile data," in *Proc. IEEE Int. Conf. Robot. Autom.*, 2014, pp. 2262–2269.
[38] B. Calli, A. Walsman, A. Singh, S. Srinivasa, P. Abbeel, and A. M. Dollar, "Benchmarking in manipulation research: The YCB object and model set and benchmarking protocols," *IEEE Robot. Autom. Mag.*, pp. 36–52, Sep. 2015.
[39] Tin Kam Ho, "Random decision forests," in *Proc. 3rd Int. Conf. Document Anal. Recog.*, vol. 1, 1995, pp. 278–282.
[40] L. Breiman, "Random forests," *Mach. Learning*, vol. 45, no. 1, pp. 5–32, 2001.
[41] L. U. Odhner and A. M. Dollar, "The smooth curvature model: An efficient representation of Euler-Bernoulli flexures as robot joints," *IEEE Trans. Robot.*, vol. 28, no. 4, pp. 761–772, Aug. 2012.
[42] R. Suárez, M. Roa, J. Cornella, and J. Cornell, "Grasp quality measures," Institut d'Organització i Control de Sistemes Ind., Universitat Politècnica de Catalunya, Barcelona, Spain, Tech. Rep. IOC-DT-P 2006-10, 2006.
[43] S. Theodoridis and K. Koutroumbas, *Pattern Recognition*, Academic Press, vol. 4, 2008.

Adam J. Spiers received the BSc degree in cybernetics and control engineering and the MSc degree in engineering and information sciences from the University of Reading, United Kingdom. He received the PhD degree in mechanical engineering from Bristol University, United Kingdom. He conducted three years of postdoctoral research in medical robotics and haptics at Bristol Robotics Laboratory in the University of the West of England, United Kingdom. He is currently an associate research scientist with the GRAB Lab, Department of Mechanical Engineering and Materials Science, Yale University, New Haven, CT. His current research focuses on human motion, robot grasping, prosthetics, and haptic navigation interfaces. He is a member of the IEEE.

Minas V. Liarokapis received the MSc degree in computer engineering from the University of Patras, Greece, the MSc degree in information technologies in medicine and biology from the National Kapodistrian University of Athens, Greece, and the PhD degree in mechanical engineering from the National Technical University of Athens, Greece. He is currently a postdoctoral associate with the GRAB Lab, Department of Mechanical Engineering and Materials Science, Yale University, New Haven, CT. His current research focuses on robust grasping and dexterous manipulation with adaptive, underactuated and compliant robot hands, as well as on robot hands design. He is a member of the IEEE.

Berk Calli received the BS and MS degrees in mechatronic program from Sabanci University, Turkey. His master thesis was on integrated visual servoing and force control algorithms for robotic manipulation. He received the PhD degree from Delft University of Technology in 2015. His thesis was on viewpoint optimization for vision-based robotic grasping. He is currently at Yale University's GRAB Lab on vision-based manipulation, dexterous manipulation, and manipulation benchmarking. He is a member of the IEEE.

Aaron M. Dollar received the BS degree in mechanical engineering from the University of Massachusetts at Amherst. He received the SM and PhD degrees in engineering sciences from Harvard, and conducted two years of postdoctoral research at the MIT Media Lab. He is currently the John J. Lee associate professor of mechanical engineering and materials science at Yale. His research topics include human and robotic grasping and dexterous manipulation, mechanisms and machine design, and assistive and rehabilitation devices including upper-limb prosthetics and lower-limb orthoses. He received the 2013 DARPA Young Faculty Award, 2011 AFOSR Young Investigator Award, the 2010 Technology Review TR35 Young Innovator Award, and the 2010 US National Science Foundation (NSF) CAREER Award. He is a senior member of the IEEE.